Journal of Materials Chemistry C

Ferroelastic Domains and Phase Transitions in Organic-Inorganic Hybrid Perovskite $CH_3NH_3PbBr_3$

Journal:	*Journal of Materials Chemistry C*
Manuscript ID	TC-ART-11-2020-005618.R1
Article Type:	Paper
Date Submitted by the Author:	28-Jan-2021
Complete List of Authors:	Bari, Maryam; Simon Fraser University, Chemistry Bokov , Alexei; Simon Fraser University, Department of Chemistry and 4D LABS Ye, Zuo-Guang; Simon Fraser University, Chemistry

ARTICLE

Ferroelastic Domains and Phase Transitions in Organic-Inorganic Hybrid Perovskite $CH_3NH_3PbBr_3$

Received 00th January 20xx,
Accepted 00th January 20xx

DOI: 10.1039/x0xx00000x

Maryam Bari♣ [a], Alexei A. Bokov♣[a]* and Zuo-Guang Ye [a]*

The high performance of $CH_3NH_3PbX_3$ (X = I, Br, and Cl) perovskites in the photovoltaics and optoelectronics has been suggested to be associated to phase symmetry and the possible existence of ferroelectricity. The accurate characterization of their crystal structures has been hampered due to the structural complexities, soft chemical bonding, and dense twinning in crystals. Here, we precisely determine the crystal symmetries and phase transitions via in-situ observations of the $MAPbBr_3$ crystals between 80 K and 500 K using polarized light microscopy and temperature-dependent measurements of dielectric properties. The phase transitions are found to occur at 237 K, 152 K and 148 K, from cubic (α) → tetragonal (β) → orthorhombic (β') → orthorhombic (γ) phases, respectively. This new sequence of phases is different from the one previously published based on diffraction methods. Characteristic twin domains are discovered in the β, β', and γ phases. Application of an external electric field does not change the domain structure, which rules out ferroelectricity. However, Joule heating can raise the temperature of the crystal by dozens of degrees, induce a phase transition and change irreversibly the domain structure and properties. The domain structure changes also under external stress, proving that the twins are ferroelastic domains. Our results suggest that elastic stress-mediated domain engineering may serve as a useful tool for tuning the microstructure by eliminating/modifying the domain walls, which may ultimately improve the stability and optoelectronic properties of halide perovskites.

Introduction

Organic-inorganic hybrid halide perovskites $MAPbX_3$ ($MA=CH_3NH_3$; X= I, Br, Cl) have been the main subject of interest for photovoltaics in the last decade, due to their exceptional properties such as high optical absorption,[1,2] high charge mobility[3] and separation,[4] large electrostriction[5], low defect density[6], and cost-effective solution-processing method.[7] They have become competitive optoelectronic materials for applications in photodetectors,[8] light-emitting diodes,[9] lasing,[10] and nonlinear absorbers,[11] micro-electromechanical actuators[5] and photocatalysts.[12] While the device technology of halide perovskites has significantly evolved in the recent years, their poor long-term stability is still of primary concern. Moreover, the origin of their physical properties has not been well understood yet. For instance, it was believed that ferroelectric domains in $MAPbX_3$ contributed to their outstanding photovoltaic performance.[13,14] However, the nature of twin domains observed in these materials remains debatable. In tetragonal phase of $MAPbI_3$, ferroelectric domains were postulated based on piezoresponse force microscopy (PFM) imaging,[15,16] but surface artifacts such as MA ionic migration and charge trapping could be misinterpreted as ferroelectric signals in PFM.[17-19] Crystallographic twin domains in $MAPbI_3$ were also observed using transmission electron microscopy[20] and reflection light microscopy,[21] and were argued to be ferroelastic (i.e. non-polar).[21] Several investigations aimed at finding ferroelectric properties in $MAPbI_3$ have failed to distinguish ferroelectric from ferroelastic domains.[22-26] Ferroelectricity can be, in principle, verified based on structural data as ferroelectrics must possess a polar space group. In particular, ferroelectricity would be permitted in the tetragonal phase with polar *I4cm* space group found in $MAPbI_3$ based on single-crystal and powder X-ray diffractions.[27,28] However, other X-ray and neutron diffraction studies revealed the *I4/mcm* symmetry,[29-31] which does not allow ferroelectricity.

In another hybrid perovskite compound $MAPbBr_3$ (which is studied in the present work), the coexistence of domains of ferroelectric and antiferroelectric nature was found in the orthorhombic phase using scanning tunnelling microscopy, but those domains were attributed to the modified arrangement of atoms/molecules at the surface and were not verified in the crystal bulk.[32] Recently, the ferroelectricity in $MAPbBr_3$ was suggested through the observation of the butterfly-like dependences of dielectric constant on bias electric field, the switchable pyroelectric-like current direction under poling voltage, and the polarization-electric field (P-E) hysteresis

[a] *Department of Chemistry and 4D LABS, Simon Fraser University, Burnaby, British Columbia, V5A 1S6, Canada*
♣These authors contributed equally to this work.
*Corresponding Authors. E-mails: zye@sfu.ca and abokov@sfu.ca
Electronic Supplementary Information (ESI) available: [details of any supplementary information available should be included here]. See DOI: 10.1039/x0xx00000x

loops.[33] On the other hand, similar current and P-E loops were interpreted to result from a special configuration of ferroelastic domains and a large conductivity, respectively, rather than from ferroelectricity.[34,35]

All these conflicting reports point to the difficulty in accurately determining the crystal symmetry and the nature of twin domains in halide perovskites, which appear to play a key role in understanding the optoelectronic properties responsible for slow carrier recombination, fast charge transport, and superior energy conversion.[13,31,36-38] Various techniques have been used to characterize the macroscopic crystal structure of $MAPbX_3$, including powder X-ray diffraction (PXRD),[28-30] single crystal X-ray diffraction (SXRD),[27,39] neutron powder diffraction (NPD),[31,40] synchrotron powder X-ray diffraction (SPXRD)[41,42] and polarized light microscopy (PLM).[21,43] The crystals were found to undergo a sequence of phase transitions upon cooling. We denote the phases observed at highest and lowest temperatures as α and γ phase, respectively.

In $MAPbI_3$ and $MAPbCl_3$ only one phase (β phase) is observed between α and γ, while in $MAPbBr_3$ there are two intermediate phases (β and β'). We denote the temperatures of transition from α to β, from β to β' and from β (or β') to γ as T_α, T_β and T_γ, respectively. The crystallographic data and transition temperatures reported for $MAPbX_3$ in the literature are collected in Table 1. Most structural investigations showed that in all $MAPbX_3$ perovskites α phase is cubic (C), β and β' phases are tetragonal (T) and two variants of orthorhombic structure were observed in the low-temperature γ phase: O_S (in $MAPbI_3$ and $MAPbBr_3$) or O_P (in $MAPbCl_3$), in which the twofold symmetry axis is along the face diagonal and one of the edges of the parent perovskite cell, respectively. However, the space groups reported by different researchers are often inconsistent with each other and incommensurate (IC) structural modulations were found in some cases. Furthermore, for $MAPbI_3$ the T or rhombohedral crystal system for the α phase and the monoclinic system for the γ phase was reported. We have recently resolved[43] the symmetry of β phase in $MAPbCl_3$ to be orthorhombic, but not tetragonal as previously believed, by means of PLM technique, which provides a more accurate determination of the crystal system than the diffraction methods do.

Especially controversial is the phase transition sequence in $MAPbBr_3$, where an additional tetragonal β' phase has been reported in a narrow temperature range of several degrees. The existence of this phase was confirmed by several experimental techniques, including differential scanning calorimetry (DSC),[35,44] NMR,[44,45] dielectric measurements,[34,35,46] Raman spectroscopy,[47,48] and neutron scattering (NS).[49,50] However, reliable information about the β' structure is still limited. Early PXRD work[29] reported the tetragonal *P4/mmm* space group with one formula unit per cell (Z=1), which implies a transition between two tetragonal phases at T_β. However, in the temperature dependent XRD and NPD studies,[40,47,51] this transition was not found. In SXRD experiments[52] superstructure reflections were observed in the β' phase, which are incompatible with a primitive (Z=1) cell. Therefore, it was suggested that the structure of the β' phase is incommensurate,[49,50] while the average symmetry is tetragonal.[50] There were also reports on the coexistence of T and O phases below 145 K (the space groups were not determined),[51] and on the presence of an incommensurate O structure in the temperature interval of several degrees between the T and commensurate O phases.[47] For the orthorhombic γ phase of $MAPbBr_3$, the centrosymmetric *Pnma* and the polar $Pna2_1$ space groups have been reported (see Table 1). Therefore, the crystal systems and space groups of different phases, and the sequence and temperatures of phase transitions in $MAPbBr_3$ are controversial. The question on whether ferroelectricity exists remains open.

The main reason for the controversy among the published crystallographic data is that the diffraction techniques are unreliable for structural characterization of hybrid perovskites due to the difficulties in detecting the positions of light atoms (H and N) in the presence of heavy lead and halogen atoms.[36,37] Another inherent problem is the dense twinning in the real crystals.[39,53] To overcome the drawbacks of the diffraction methods, we apply in this work polarized light microscopy to determine accurately the phase symmetry and to resolve the issue concerning ferroelasticity or ferroelectricity in $MAPbBr_3$. PLM is a convenient and powerful research tool for determining the phase symmetry by analysing the twin domains and domain structures. In addition, ferroelasticity or ferroelectricity can be identified through evolution of domain structure driven by an external elastic or electric field, respectively. We find, in particular, that similar to $MAPbCl_3$ crystals investigated using the same approach in our previous work,[43] the $MAPbBr_3$ crystals are ferroelastic, but not ferroelectric. Through this work, the prominent advantages of PLM approach are highlighted for the determination of the crystal structures, phase transition temperatures, and domain behaviour.

Results and discussion

Crystal Structure at Room Temperature and Phase Transitions. Fig. 1a shows the powder X-ray diffraction pattern of $MAPbBr_3$ at room temperature. Pawley refinement yielded a perovskite structure of cubic symmetry with the space group of $Pm\bar{3}m$ and lattice parameter of a = 5.918Å, which is consistent with the previous reports.[29,39] The temperature dependence of dielectric constant shown in Fig. 1b reveals the phase transitions in $MAPbBr_3$. Upon cooling, the dielectric constant increases monotonically down to 152 K, but a very small anomaly is observed at the temperature of 237 K, corresponding to the transition from α to β phase (see the inset of Fig. 1b). A sharp peak at 152 K indicates the $\beta \rightarrow \beta'$ transition, and a significant drop in the dielectric constant at 148 K signifies the $\beta' \rightarrow \gamma$ transition. The observed phase transition temperatures are in good agreement with the previous measurements (see Table 1).

Crystal Symmetry and Domain Structure Characterized by Polarized Light Microscopy. A brief explanation of optical crystallography principles which are used for interpreting the PLM observations in our work can be found in Ref. 43. Here,

Table 1. Summary of the crystal structures and phase transition temperatures for $MAPbX_3$ (X = I, Br, Cl).

Composition	α	T_α (K)	β	T_β (K)	β'	T_γ (K)	γ	Technique
$CH_3NH_3PbI_3$		326-331			-	162		DSC,[30,35,44,54] Dielectric data,[35,46] NMR[45]
	C ($Pm\bar{3}m$)		T (*I4/mcm*)				O_S (*Pna2₁*)	PXRD[29]
	C ($Pm\bar{3}m$)		T (*I4/mcm*, Z=4)					SXRD,[55] PXRD[30]
			T (*I4/m*)				O_S (*Pnma*, Z=4)	SXRD[30]
	T (*P4mm*, Z=1)		T (*I4cm*, Z=4)				Monoclinic	SXRD,[27,28] PXRD[28]
	C ($Pm\bar{3}m$)		T (*I4/mcm*)				O_S (*Pnma*, Z=4)	NPD,[31] SPXRD,[41] SXRD[54]
	T (*P4mm*, Z=1) or Rhombohedral							SXRD[39]
$CH_3NH_3PbBr_3$		230-237		150-156		146-149		Dielectric data,[34,35,46] NMR,[44,45] DSC,[35,44] NS[49,50]
	C ($Pm\bar{3}m$)		T (*I4/mcm*, Z=4))		T (*P4/mmm*, Z=1)		O_S (*Pna*2$_1$)	PXRD[29]
	C ($Pm\bar{3}m$)							SXRD,[39,56]
	C (P$\bar{4}$3m)							SXRD,[39,56]
	C ($Pm\bar{3}m$)				superstructure			SXRD[52]
	C ($Pm\bar{3}m$)		T (*I4/mcm*, Z=4)					SSXRD,[57] SPXRD[42]
	C ($Pm\bar{3}m$)		T (*I4/mcm*)				O_S (*Pnma*, Z=4)	PXRD & NNPD,[40] SPXRD[58]
			T (*I4/mcm*, Z=4)				O_S (*Pnma*); O_S (*Imma*, IC); at T>140K	SXRD[47]
	C		T		T		O + T	SXRD & PXRD[51]
	C		T		T		O	SXRD[47]
	C ($Pm\bar{3}m$)		T		Os		O_S	PLM This work
$CH_3NH_3PbCl_3$		178				172		NMR,[45] Dielectric data,[35,46] DSC,[35,44]
	C ($Pm\bar{3}m$)		T (*P4/mmm*, Z=1)				O_P (*P222₁*, Z=2)	PXRD[29]
	C ($Pm\bar{3}m$)		T (IC)				O_P (*P2₁2₁2₁*, Z= 8)	SXRD[53]
							O_P (*Pnma*, Z=8)	SPXRD &NPD[59]
	C ($Pm\bar{3}m$)							SXRD,[60] PXRD &NPD[39]
	C ($Pm\bar{3}m$)		O_S				O_P	PLM[43]

the extinction directions (characterized by an angle δ which is defined as the angle between the privilege direction of the polarizer and the <100> direction of the parent cubic phase) and the orientations of ferroelastic domain walls (characterized by angle *φ* which is defined as the angle between the domain wall trace on the crystal surface and the <100> direction of the parent cubic phase) are the main parameters to determine the crystal symmetry. The values of δ and φ theoretically possible in different crystal phases are listed for convenience in Supporting Information, Table S1. Fig. 2a demonstrates that at room temperature, the (001) crystal is in extinction at any arbitrary position δ. The same behaviour is observed on the (110) and (111) crystal plates at all temperatures T > Tα (= 237 K), indicating that in the α phase, the crystal is optically isotropic. Fig. 2b shows the PLM image

taken with a first-order red plate (λ = 530 nm) placed between the sample and analyser to differentiate the extinct areas from possible opaque inclusions visually. The crystal in complete extinction has the same (zero) retardation as the background and exhibits almost the same (magenta) colour as in its surrounding (Note that magenta colour is expected for isotropic colourless crystals, but due to the orange colour of $MAPbBr_3$, the crystal does not show exactly a magenta colour). Some areas of the crystal remain black with the superimposed first-order red plate, which indicates that these are opaque inclusions. The absence of birefringence confirms the cubic symmetry of α phase, which agrees with our PXRD analysis and previous diffraction studies.

The PLM image of the β phase in a thin as-grown (001) crystal which has not been polished is shown in Fig. 3a. When the crossed polarizers are at the angles of δ = ± 45° to the <100> directions, the crystal is bright, while at δ = 0° or 90° it is in extinction (completely black) as shown in the inset of Fig. 3a. Complex patterns of irregular lines are visible (some of them are marked by white arrows) which remain unchanged at all the studied temperatures between 80 and 500 K. These uneven patterns are mostly due to the etching of the crystal surface by the residual solvent after the crystal was pulled out of the growth solution.

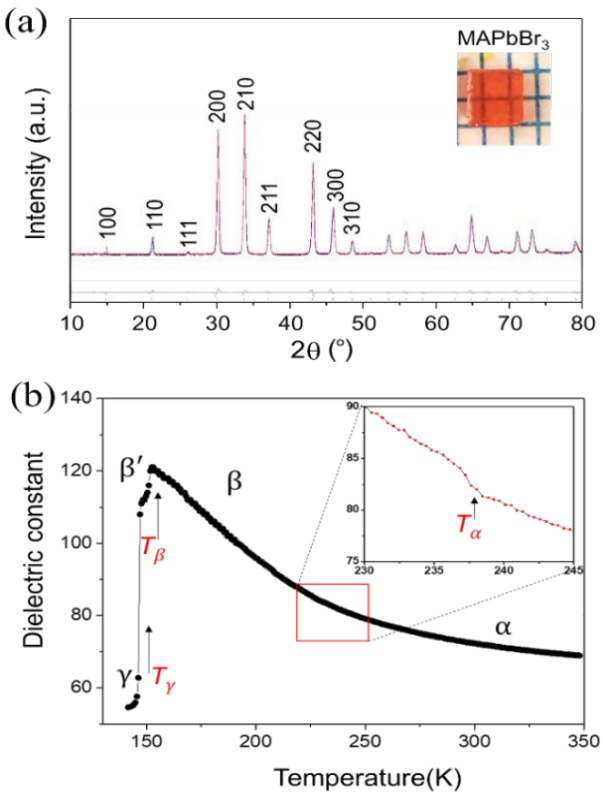

Fig. 1 (a) Powder X-ray diffraction pattern of $MAPbBr_3$ at room temperature indexed according to the cubic $Pm\bar{3}m$ symmetry (blue line), the refinement (red line), and the difference (grey line at the bottom of the panel). (b) Temperature dependence of the dielectric constant measured on a (001) plate at the frequency of 100 kHz, revealing the transitions from the α to β phase at T_α, from β to β' phase at T_β and from β' to γ phase at T_γ.

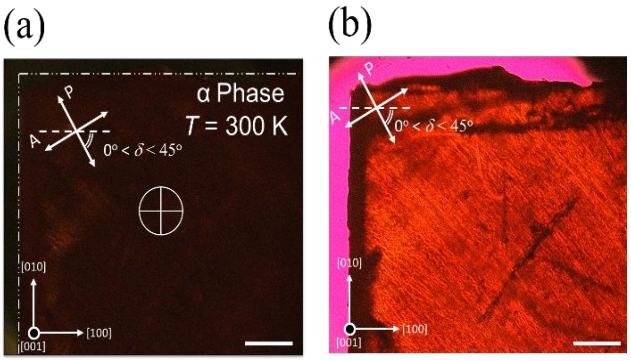

Fig. 2 (a) PLM image of a (001) plate of $MAPbBr_3$ (thickness~ 0.2 mm) in the α phase with the crossed polarizers directed at an arbitrary δ. (b) The same crystal when a first-order red plate is superimposed. The temperature and the directions of crystallographic axes, indicatrix axis and polarizers are shown; scale bars = 200 μm.

One can also observe the straight walls aligned in the <110> directions (i. e. walls with φ = 45°), which separate fine lamellar twin domains with a width of less than 5 μm. In T phase (expected based on the published diffraction studies) the axes of optical indicatrix of these domains should be mutually perpendicular (walls between such domains are called 90° walls). There are also a few large domains with a size of more than 100 μm (see the sketch in Fig. 3a). The same values of δ and φ were observed in the β phase of other small as-grown crystals which we studied. However, these values may correspond to any symmetry listed in Table 1S, except rhombohedral (R).

To determine the symmetry of the β phase unambiguously, we then investigate larger crystals. In these cases, it was necessary to polish the crystal in order to reduce the thickness so as to obtain a sample transparent enough for optical study. Fig. 3b, c shows such a (001) crystal. Polishing resulted in clearly visible scratches on the crystal surface and internal strains that make the domain walls slightly blurry. The extinction of the whole sample occurs when the crossed polarizers angle is δ = 0°/90° (inset in Fig. 3b). A comparatively large square region in the centre of the crystal appears to be in extinction (black) at any angle δ. When a first-order red plate is superimposed, this region becomes bright (Fig. 3c), which proves that it is a transparent region and that it is a domain whose optical axis is perpendicular to the surface of the crystal plate. The domains with the optical axis perpendicular to (001) plate are known as c-domains, and they are possible only in a tetragonal phase (see Table 1S). They should be separated from the domains having optical axis parallel to (001) plate (the so-called a-domains) by 90° walls which are inclined to the surface by an angle of 45° and whose intersections with the surface are along <100> (i.e., φ = 0° or 90°).[61] Such walls are shown in blue in the sketch of Fig. 3c. Four a-domains in the crystal are separated by the 90° walls (yellow walls in the sketch) perpendicular to the crystal surface.

Therefore, the observed domain structure unambiguously indicates the T symmetry for the β phase, which is consistent with the symmetry deduced from X-ray and neutron

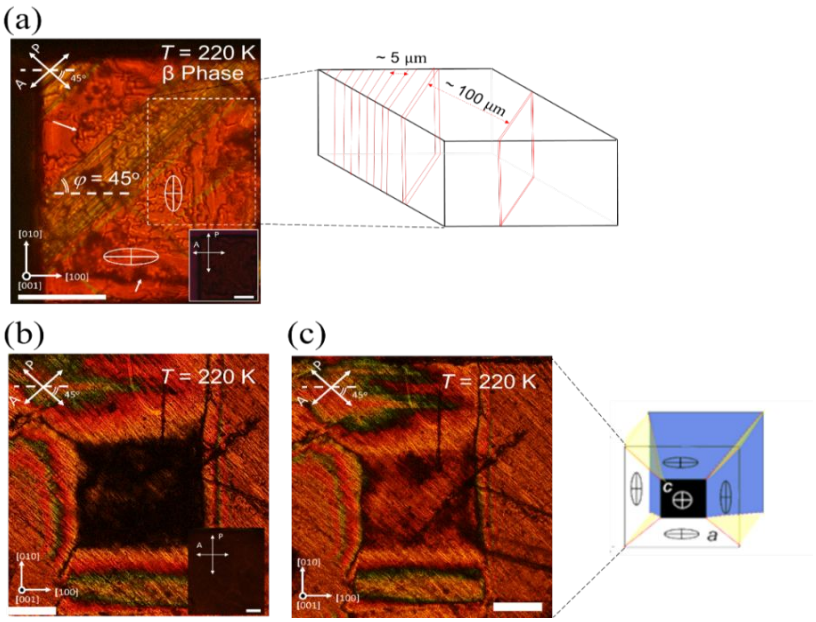

Fig. 3 PLM images of (001) oriented $MAPbBr_3$ crystal plates in the β phase. (a) An as-grown crystal with a thickness of ~ 80 μm observed at $\delta = 45°$, and at $\delta = 0$ (in the inset). The sketch shows the arrangement of 90° walls between a-domains in the area delimited by the dashed box. (b, c) A polished crystal with a thickness of ~ 200 μm observed at (b) $\delta = 45°$, and $\delta = 0$ (in the inset), and (c) with the first-order red plate at $\delta = 45°$. The sketch shows the domain structure and directions of indicatrices in different domains. The 90° walls between a-domains are highlighted in yellow; the 90° walls between a- and c-domains are highlighted in blue. The temperature, the directions of crystallographic axes of the parent cubic phase, the directions of polarizers, and the angles (δ, φ) are indicated; scale bars = 200 μm.

diffraction data (Table 1). Other examples of domain structures in the (110) and (111)-oriented plates that are consistent with the T symmetry for the β phase are provided in Supplementary Information, Fig. S1.

The domain structure does not change when the temperature varies within the range of β phase, but below the temperature of $T_\beta = 152$ K, some regions with extinction at $\delta = 45°$ may appear, and after rotating the polarizers to $\delta = 0°$ they become bright (Fig. 4). The observed extinction behaviour is incompatible with the T, O_P and R phases but only permitted by the O_S symmetry (see Table S1). The crystal plate presented in Fig. 4 consists of two wedge-shaped domains separated by the (011) wall, as shown schematically in Fig. 4c. The lower part of the crystal remains without extinction at any position of polarizers due to the superimposed O_S domains having different vibration directions orientated along <110> and <001>, respectively. The entire upper part has vibration directions along <110> and, consequently, appears with extinction at $\delta = 45°$. A multicoloured strip-like interference pattern observed in the lower part of the crystal is due to the wedge-shaped morphology of domains. At $\delta = 45°$, the upper wedge (domain) in Fig. 4c is in extinction and, therefore, it does not contribute to optical retardation. The interference strips in this case are created by the retardation of the lower wedge. At $\delta = 0°$, the lower wedge is in extinction and the interference strips come from the upper wedge. These two interference pictures are different because the corresponding wedges are observed in different crystallographic directions and, therefore, their effective birefringences (which are proportional to the retardations) are different.

To further confirm the O_S symmetry of the β' phase, another crystal is examined, which is shown in Fig. 5a-b. The extinction appears in most regions of the crystal when the crossed polarizers are at $\delta = 0°$, and it becomes completely bright at $\delta = 45°$. Some regions in Fig. 5a are bright at both $\delta = 0°$ and 45°, indicating that two or more domains with nonparallel vibration directions overlap. This is another solid confirmation of the O_S symmetry, similar to the discussion in the previous paragraph. Some domain wall traces are measured to be at $\varphi \approx 0/90°$ and 45°, i.e., orientated along the <100> and <110> directions, as marked in the enlarged regions in Fig. 5a. These angles are possible in any phase, according to Table S1. However, some walls form an angle of $\varphi \approx 15°$. These so-called S-walls are allowed in the O_S phase only (see Table 1S). Thus, the observed extinction positions and directions of domain walls are fully compatible with the orthorhombic (O_S) symmetry.

During the transition from the β' to γ phase upon further cooling, we observed a significant change of domain structure at the phase transition temperature, T_γ (148 K). Fig. 5 illustrates such a change showing the crystal before (panels a and b), and after (panels c and d) the transition

(like in β phase, we never noticed a variation of domain structure at temperatures other than the phase transition temperatures). In the γ phase, some parts of the sample are in extinction at $\delta = 0°$, and some other parts at $\delta = 45°$, while most regions remain bright at any δ. As discussed above, this confirms the O_S symmetry, similar to β' phase. The significant change of domain structure at T_γ can be associated with macroscopic internal stresses during the transition which were caused by

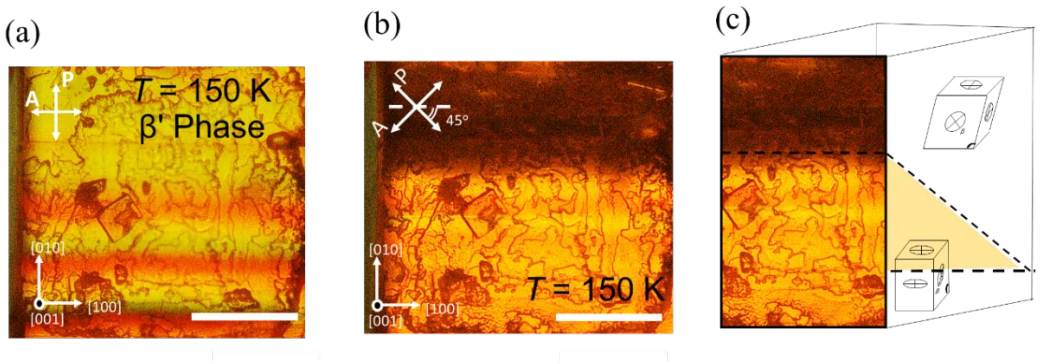

Fig. 4 PLM images of the same as-grown (001) crystal as in Fig. 3a observed in the β' phase at (a) $\delta = 0°$ and (b) $\delta = 45°$. (c) Schematics of domain configuration, where the inclined domain wall is highlighted by the yellow plane with dashed lines. The monoclinic distortion of the parent cubic structure in two adjacent O_S domains and the orientations of indicatrix in these domains are also shown. The temperature, the directions of crystallographic axes, and the positions of polarizers are indicated; scale bar = 100 μm.

the differences in lattice parameters between the two O_S phases. Previously, XRD analysis[29] revealed an orthorhombic O_S symmetry with a polar space group of *Pna2₁*, and other reports assigned a non-polar group of *Pnma*[25,40,47] to the γ phase. Here, we confirm the orthorhombic O_S symmetry, however, the space group cannot be determined from PLM analysis.

Note that the existence of phases of lower (monoclinic or triclinic) symmetry in $MAPbBr_3$ can be unambiguously excludes based on our observations. In a triclinic phase, the extinctions should be observed only at angles other than $\delta =$ 0°/90° or $\delta = \pm 45°$. In a monoclinic phase, two variants are possible in a (001) oriented crystal:[62] i) coexistence of the δ = 0°/90° domains and the domains having arbitrary, but different from 0°/90° or ± 45°, values of δ; and ii) coexistence of the $\delta = \pm 45°$ domains and the domains having arbitrary, but different from 0°/90° or ± 45°, values of δ. The coexistence of the domains with $\delta = \pm 45°$ and $\delta =$ 0°/90°, which we have observed in the β' and γ phases, and the existence of c-domains observed in the β phase, are not permitted in the monoclinic crystal system.

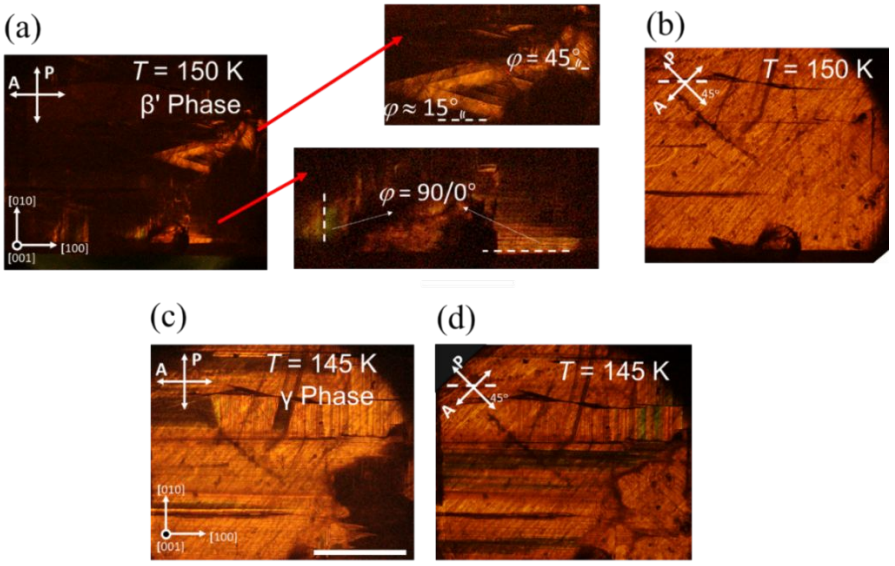

Fig. 5 PLM images of a polished (001) $MAPbBr_3$ crystal after cooling to the β' phase (a, b), and further to the γ phase (c, d) with crossed polarizers at $\delta = 0°$ (a, c) and at $\delta = 45°$ (b, d). The enlarged areas presented in panel (a) demonstrate the domain wall directions. The temperature and the directions of crystallographic axes are indicated; scale bars = 400 μm.

Therefore, our investigation confirms the crystal classes of the α, β and γ phases previously reported based on diffraction studies. However, the symmetry of the β' phase is found to be orthorhombic, but not tetragonal, as previously thought. Note that an IC phase with O_S *Imma* symmetry was observed[47] by SXRD in the narrow temperature interval around T ~ 150 K between the O_S *Pnma* and T phases. Our results suggest that this orthorhombic IC phase can be just the β' phase observed by other authors.

Search for ferroelectricity in $MAPbBr_3$. To search for ferroelectricity in $MAPbBr_3$, we have performed PLM observation of the domain structure under an electric field. In principle, applying an electric field larger than the coercive field must result in changes in the domain configuration in ferroelectric materials, which is due to the reorientation of the spontaneous dipole moments in the direction prescribed by the applied field. The schematics of the experimental setup is shown in Fig. 6a. Fig. 6b-c demonstrates that the domain structure of the β phase does not change under an electric field below about 8 kV cm^{-1}. But under a field of $E \geq$ 8 kV cm^{-1} applied for several seconds or longer, the crystal becomes black at any position of polarizers (see Fig. 6d) while remaining fully transparent (see inset in Fig. 6d). This behaviour cannot be explained by ferroelectric domain switching, as under the used conditions (the electric field is applied parallel to [100]), the switching should result in the development of a-domain which have extinction only at δ = 0°/90°. In fact, the T phase transforms under the field into a phase which is optically isotropic. The development of the phase front between T and isotropic phases with time is demonstrated in Supplementary Movie S1. This behaviour seemingly contradicts the Curie's principle which, when applied to crystal physics, states[63] that a crystal under an external influence will exhibit only those symmetry elements that are common to the crystal without the influence and the influence without the crystal. To resolve the paradox, the current generated by the field of 8 kV cm^{-1} at two temperatures, 230 K and 190 K, is recorded as a function of time (Fig. 6f). The spike observed at the moment when the field is switched on is evidently a displacive current due to the charging of the capacitor formed by the crystal, electrodes and connecting setup. The current detected after that can be attributed to the dc conduction and slow polarization processes (if any). It increases with time, which can be explained by Joule heating of the crystal, resulting in an increase in conductivity and thereby further heating. The transition to the isotropic phase starts in t_s =22 seconds after switching on the field at temperature T_1=230 K, and in t_s = 38 s at T_1 = 190 K, showing that a longer time is needed for the phase transition to occur when the sample is cooled at a lower temperature.

The amount of heat needed to change the temperature of the crystal from T_1 to the transition temperature T_α = 237 K, assuming that the crystal is thermally isolated and its heat capacity is constant, can be calculated as:

$$Q_{\mathrm{h}} = C(T_\alpha - T_1)V/(vN_{\mathrm{A}}), \quad (1)$$

where C is the molar heat capacity (which changes insignificantly between 170 and 200 J K^{-1} mol^{-1} in the temperature range of consideration according to Ref. 64), V is the volume of the crystal (1.2 mm^3 in our experiment), $v \approx 2.1\times10^{-19}$ mm^3 is the volume of the perovskite unit cell and $N_A = 6.02\times10^{23}$ mol^{-1} is the Avogadro constant.

Joule heat (Q_J) generated by a time-dependent current (I) in the interval of time, t_1 and t_2, is given by:

$$Q_J = U\int_{t_1}^{t_2} I(t)dt, \quad (2)$$

where U is the applied voltage (400 V in our experiment). Applying this equation with t_1=0 and t_1=t_s, we calculate the integral numerically as the area under the $I(t)$ curves in Fig. 6f, and obtain Q_J = 0.041 J for T_1 = 230 K and Q_J = 0.12 J for T_1 = 190 K. These values are significantly larger than $Q_h \approx$ 0.014 J and $Q_h \approx$ 0.08 J calculated from Eq. 1 for T_1 = 230 K and 190 K, respectively, indicating that Joule heat generated is large enough to heat the crystal up to the phase transition temperature. The difference $Q_J - Q_h$ is evidently dissipated to the environment (sample chamber).

When the temperature of the crystal reaches the transition temperature at t = t_s, the generated Joule heat must be greater than the latent heat of the first order transition for the crystal to transform completely into the high-temperature cubic phase. The temperature of the crystal should not change during the transition and the latent heat can be calculated as $Q_{\mathrm{tr}} = \Delta^{H_{\mathrm{tr}}V}/(vN_{\mathrm{A}})$ = 0.009 J, where ΔH_{tr} is the molar enthalpy of transition (951 J.mol^{-1} according to Ref. 44). This value of Q_{tr} is indeed significantly less than Q_J = 0.086 J for T_1 = 230 K and Q_J = 0.26 J for T_1 = 190 K calculated from Eq. (2) in the time interval between t_s and the moment when the transition is practically finished (t_f), confirming that enough Joule heat is generated to induce the phase transition.

Note in Fig. 6f that, some time before and after the moment t_f is reached, the current remains almost unchanged, only slightly fluctuating around a constant value (~ 40 μA for T_1 = 190 K, which corresponds to the maximum current density of ~ 6 mA/cm^2). This suggests that thermal equilibrium is established between the heating from the current and the cooling from the environment, and the crystal temperature is stabilized in the α phase very close to T_α. The probable reason for the current fluctuation could be attributed to the dynamic process of the crystal reaching the thermal equilibrium in which the momentary decrease of crystal temperature results in the transition of a small part of the crystal into the T phase, while the release of the associated latent heat in turn heats the crystal back into the cubic phase. This process can be visualized by the corresponding small fluctuations of the phase boundary position shown in Supplementary Movie S1.

The crystal becomes birefringent again, and the crystal symmetry appears to be tetragonal with a different domain structure after the field is removed, as shown in Fig. 6e. Note that this change in the domain structure is the result of phase transition but not the direct effect of the electric field. Thus, an

electric field does not change the domain structure, which proves the absence of ferroelectricity in the β phase. Note also that the observed behaviour can be related to the fact that the organic-inorganic hybrid perovskites have an ultra-low thermal conductivity,[65,66] which impedes the dissipation of the Joule heat from the crystal into the environment.

Joule heating has been proposed as one of the major contributors to energy loss in perovskite solar cells.[67] It also causes the external quantum efficiency roll-off in perovskite light-emitting diodes (LEDs)[68,69] and inhibits practical realization of electrically driven laser diodes[70]. It has been reported that a current density of a few mA cm^{-2} (i. e. comparable to those observed in our experiments) can result in an irreversible decrease of perovskite LEDs performance.[71] Our PLM observations clearly show that Joule heating in halide perovskites, particularly in $MAPbBr_3$, should be taken into account when interpreting the experimental results involving a considerable electric current density. It can not only heat up the material by dozens of degrees, but also lead to phase transitions and changes in the twin domain structure and, consequently, the properties of the material.

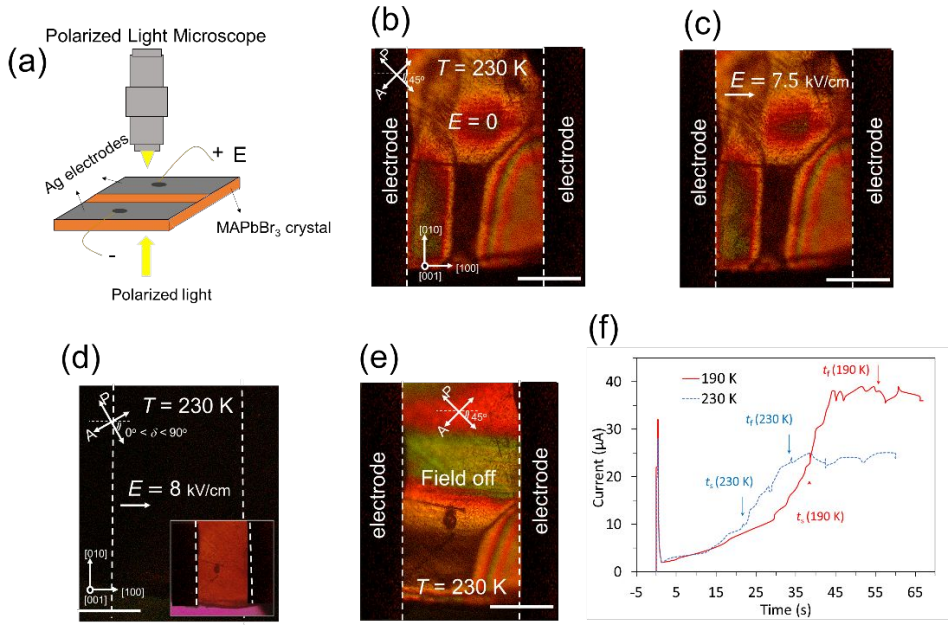

Fig. 6 Investigation of the effect of an applied electric field on the twin domains in β phase of $MAPbBr_3$ crystal. (a) Schematic drawing of the experimental setup. (b-c) PLM images of the (001) crystal with a thickness of 150 μm before (b) and after the application of an electric field of E = 7.5 kV cm^{-1} (c), and E = 8 kV cm^{-1} (d) along the [100] direction. Inset in (d) shows the image taken with a first-order red plate to confirm the transparency of the crystal under the field. (e) The same crystal after the applied field of E = 8 kV cm^{-1} is switched off. (f) The current versus time measured when the field of E = 8 kV cm^{-1} is applied at the temperature T_1 = 230 K (dashed line) or T_1 = 190 K (solid line): the arrows show the start and endpoints of the electric field induced phase transition from β to α. The temperature, the directions of the crystallographic axes, the field direction, and the polarizers are indicated; scale bars = 200 μm.

The effect of the electric field is also examined in the β' and γ phases of $MAPbBr_3$ crystals using the same experimental setup shown in Fig. 6a. A DC field with a magnitude of ~ 10 kV cm^{-1} was applied at 150 K and 140 K, respectively. As can be seen from Fig. 7a-d, no change in the domain structures occurs. A larger field results in dielectric breakdown at those temperatures. At the lowest available temperature of 80 K with a higher breakdown field, the domain structure remains unchanged even at a field of ~ 15 kV cm^{-1} (see Fig. S2). This behaviour indicates that the β' and γ phases are also non-ferroelectric.

Development of Ferroelastic Domains in $MAPbBr_3$ under External Stress Application (Domain Engineering). Ferroelasticity is the result of the coexistence of different crystallographic orientation (strain) states in a crystal that can be switched from one state to another by external stress.[72] In our experiments, external stress was applied to a thin crystal (t ~ 0.1 mm) to investigate its effect on the domain structure

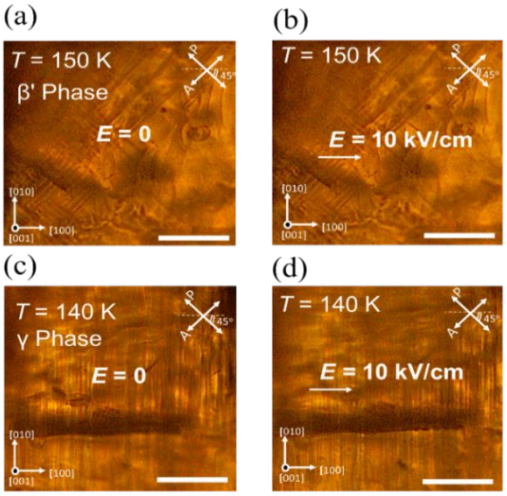

Fig. 7 PLM images of a (001) oriented $MAPbBr_3$ crystal in (a, b) β' phase and (c, d) γ phase, before (a, c) and after (b, d) application of an electric field E = 10 kV cm^{-1} along

the [100] direction. The temperature, the directions of crystallographic axes, the electric field and the polarizers are indicated; scale bars = 100 μm.

using in-situ polarized light microscopy. The experimental setup is shown in Fig. 8a. The cubic to tetragonal phase transition produces laminar fine domains with the φ = 45° orientation (Fig. 8b). The system evolves into a state with wider domains, and the domain walls disappear in some areas in response to the external stress (Fig. 8c). Likewise, two low-temperature phases (β' and γ) are examined. The domain structures can be easily changed and transformed into a new domain state (see Fig. 8d-g). These experiments show that the domains in β, β' and γ phases are clearly affected by the external stress and, therefore, these are ferroelastic domains, and $MAPbBr_3$ can be classified as ferroelastic.

It is known that the properties of ferroic materials depend largely on the presence of domain walls and their patterns.[73-75] Therefore, "domain engineering" is generally considered as a powerful approach for improving the performance of materials. Recent studies of twin domains in another hybrid halide perovskite, $MAPbI_3$, revealed the important connection between the crystal properties and its domain structure. It was shown, in particular, that ferroelastic domains modulate the intensity of light-matter interaction.[76] Ferroelastic domain boundaries were found to have negligible influence on the carrier transport across them, in contrast to regular grain boundaries which tend to block the carrier transport.[77] On the other hand, the development of the domains helps reduce strain in thin films, while strain was found to accelerate degradation of perovskite structure[78] and strain gradient coupled with chemical gradient can induce non-ferroelectric electric polarization in a centrosymmetric crystal.[79] It is expected that the ferroelastic domains in $MAPbBr_3$ could have similar effects. Moreover, our results provide a systematic analysis and comprehensive understanding of ferroelastic domains and domain structures in $MAPbBr_3$, which can apply to other halide perovskite crystals, and demonstrate that applying appropriate external stress may change the domain pattern dramatically, opening up the way to tune the opto-electronic properties by stress and to possibly realize mechano-opto-electronic effects and devices.

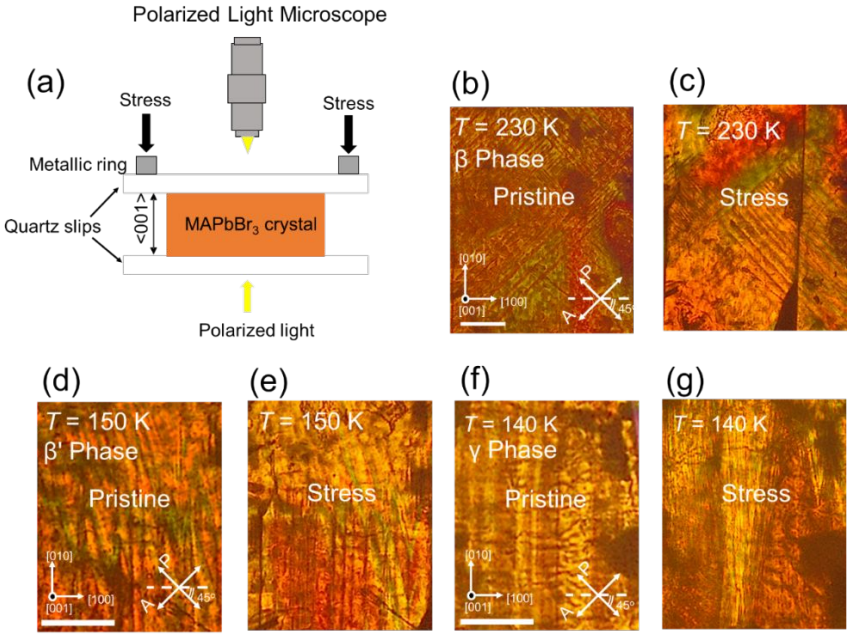

Fig. 8 Evolution of the domain structure in a (001)-oriented $MAPbBr_3$ crystal under external stress. (a) Sketch showing the application of mechanical stress in the <001> direction. (b-g) The domain structures in the β phase (b, c), β' phase (d, e) and γ phase (f, g), before (b, d, f) and after (c, e, g) the application of the stress. A first-order red plate is inserted to improve visibility of domain walls. The temperature, the directions of crystallographic axes, and polarizers are indicated; scale bars = 100 μm.

Experimental

Growth of $CH_3NH_3PbBr_3$ Crystals. Room temperature crystallization (RTC) method recently developed in our laboratory was used. Two halide precursors, CH_3NH_3Br and $PbBr_2$, were first dissolved in DMF solvent to form a homogeneous 1.5 [M] solution, which was stirred continuously at room temperature for two hours. The solution was then transferred to a half-closed vial and held for 12 hours at room temperature. Many transparent orange cuboid crystals with different sizes up to 3 mm were obtained (see e.g. Fig. 1(a), Inset).

Structural Analysis by Powder X-ray Diffraction. A fine powder was obtained by grinding several small crystals. PXRD was performed on a Rigaku Rapid Axis Diffractometer equipped with the Cu Kα radiation (λ = 1.5405 Å) at room temperature. The obtained XRD pattern was analysed by the

Pawley fitting method based on the model of cubic structure with space group of $Pm\bar{3}m$ using TOPAS software package.

Dielectric Measurements. The large opposite surfaces of (001) crystal plates were covered with silver paste to form electrodes, and gold wires were then attached to the electrodes. The relative permittivity (dielectric constant) was measured as a function of temperature at a field strength of about 5 V_{rms} mm^{-1} using a Novocontrol Alpha broadband dielectric analyser equipped with a Quatro Cryosystem for temperature control. The data were collected upon heating the specimen at the rates of 0.5 K/min between 140 K and 210 K and 1 K/min between 210 K and 350 K, respectively. The change of rate resulted in a small "anomaly" around 210 K visible in the dielectric curve presented in Fig. 2(b), which was an artifact.

Polarized Light Microscopy (PLM). Several crystals were selected for PLM examination with various thicknesses, including as-grown thin (~ 0.1 mm) plates and thicker (~ 0.2 mm) crystals which were cut parallel to the (001), (011) or (111) crystallographic planes and then polished to optical quality using silicon carbide sandpapers and lapping sheets. The PLM studies were performed using an Olympus BX60 polarizing microscope equipped with an Olympus UC 30 digital camera. A Linkam HTMS600 heating/cooling stage was used for investigations in the temperature range of 80-500 K. To differentiate small optical retardation (and thus weak colour contrast) visually, a sensitive tint plate (1λ, U-TP530, Olympus) was used. The fast and slow axes of optical indicatrix were determined with the help of a Berek compensator. To study the electric field effect, two parallel stripes made of silver paste were deposited on one of the large (001) faces of the crystal (Fig. 6a). An external dc electric field was applied along the [100] direction through two gold wires connected to the silver electrodes. The domain structure in the sample was studied by PLM under different electric fields. To apply external uniaxial stress, the (001) crystal plate was placed between two quartz slips, and the upper slip was pressed (Fig. 8a).

Conclusions

We have accurately identified the crystal symmetry for the various phases of $MAPbBr_3$ using polarized light microscopy. The crystal undergoes a sequence of phase transitions as the temperature is lowered: from cubic (α) to tetragonal (β), to side-centred orthorhombic (β'), and to another side-centred orthorhombic (γ). A summary of the crystal structure in the different phases of $MAPbX_3$ perovskites based on the PLM observations of this work and our previous work,[43] as well as the most recently published diffraction data, is presented in Fig. 9.

Various twin ferroelastic domains are found in the β, β' and γ phases of $MAPbBr_3$. The observed domain structures are found to agree with those predicted theoretically for perovskite ferroelastics. In the tetragonal β phase, the-domains are separated by 90° walls parallel to the {110} crystallographic planes. In the orthorhombic β' and γ phases, besides the {100} and {110} walls, planar S-walls are found which are not crystallographically prominent planes of fixed indices. The domain structures in the β, β' and γ phases are examined under an electric field, and no evidence of ferroelectricity is found. A large enough applied electric field results in the heating of the sample by leakage current and thereby the phase transition from T to high-temperature cubic phase.

We also provide solid evidence for ferroelasticity in the β, β' and γ phases in which the configuration of domains can be altered when the crystal is subjected to external stress. We anticipate that domain engineering by application and release of stress can resolve the key issue regarding the long-term stability of halide perovskites and point out a direction toward improving their performance.

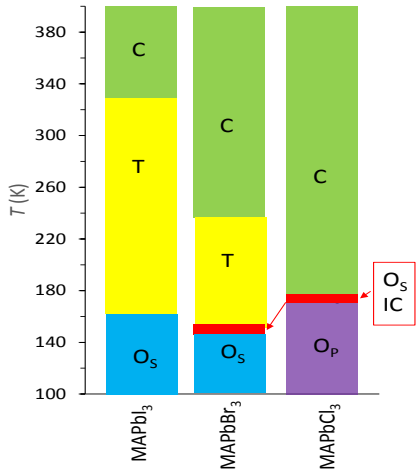

Fig. 9 Temperature intervals and crystal systems of different phases observed in $MAPbX_3$ (X = I, Br and Cl) hybrid halide perovskites.

Author Contributions

‡These authors contributed equally.

Z.-G.Y. initiated the project, obtained funding, and coordinated the research work as the PI. M.B. and A.A.B. designed and performed the experiments. The manuscript was written based on the contributions of all the authors. All the authors have given approval to the final version of the manuscript.

Conflicts of interest

There are no conflicts to declare.

Acknowledgments

This work was supported by the Natural Sciences and Engineering Research Council of Canada (NSERC, Grant No. RGPIN-2017-06915) and the U. S. Office of Naval Research (ONR, Grant No. N00014-16-1-3106).

Notes and references

1 M. A. Green, A. Ho-Baillie, H. J. Snaith, *Nat. Photonics,* 2014, **8**, 506-514.
2 Y. Lee, J. Kwon, E. Hwang, C. H. Ra, W. J. Yoo, J. H. Ahn, J. H. Park, J. H. Cho, *Adv Mater.,* 2015, **27**, 41-46.
3 C. Wehrenfennig, G. E. Eperon, M. B. Johnston, H. J. Snaith, L. M. Herz, *Adv. Mater.,* 2014, **26**, 1584-9.
4 Y. Chen, J. Peng, D. Su, X. Chen, Z. Liang, *ACS Appl. Mater. Interfaces,* 2015, **7**, 4471-4475.
5 B. Chen, T. Li, Q. Dong, E. Mosconi, J. Song, Z. Chen, Y. Deng, Y. Liu, S. Ducharme, A. Gruverman, F. Angelis, J. Huang, *Nat. Mater.,* 2018, **17**, 1020-1026.
6 D. A. Shi, R. Comin, M. Yuan, E. Alarousu, A. Buin, Y. Chen, S. Hoogland, A. Rothenberger, K. Katsiev, Y. Losovyj, X. Zhang, P. A. Dowben, O. F. Mohammed, E. H. Sargent, O. M. Bakr, *Science,* 2015, **347**, 519-522.
7 D. Liu, T. L. Kelly, *Nat. Photonics,* 2013, **8**, 133-138.
8 M. Cao, J. Tian, Z. Cai, L. Peng, L. Yang, D. Wei, *Appl. Phys. Lett.,* 2016, **109,** 233303.
9 Z. K. Tan, R. S. Moghaddam, M. L. Lai, P. Docampo, R. Higler, F. Deschler, M. Price, A. Sadhanala, L. M. Pazos, D. Credgington, F. Hanusch, T. Bein, H. J. Snaith, R. H. Friend, *Nat. Nanotechnol.,* 2014, **9**, 687-692.
10 G. Xing, N. Mathews, S. S. Lim, N. Yantara, X. Liu, D. Sabba, M. Gratzel, S. Mhaisalkar, T. C. Sum, *Nat. Mater.,* 2014, **13**, 476-480.
11 T.-C. Wei, S. Mokkapati, T.-Y. Li, C.-H. Lin, G.-R. Lin, C. Jagadish, J.-H. He, *Adv. Funct. Mater,* 2018, **28**, 1707175.
12 X. Zhu, Y. Lin, J. San Martin, Y. Sun, D. Zhu, Y. Yan, *Nat. Commun.,* 2019, **10**, 2843.
13 J. M. Frost, K. T. Butler, F. Brivio, C. H. Hendon, M. van Schilfgaarde, A. Walsh, *Nano Lett.,* 2014, **14**, 2584-2590.
14 S. Liu, F. Zheng, N. Z. Koocher, H. Takenaka, F. Wang, A. M. Rappe, *J. Phys. Chem. Lett.,* 2015, **6**, 693-699.
15 Y. Kutes, L. Ye, Y. Zhou, S. Pang, B. D. Huey, N. P. Padture, *J. Phys. Chem. Lett.,* 2014, **5**, 3335-3339.
16 D. Seol, A. Jeong, M. H. Han, S. Seo, T. S. Yoo, W. S. Choi, H. S. Jung, H. Shin, Y. Kim, *Adv. Funct. Mater,* 2017, **27**, 1702207.
17 J. M. Frost, K. T. Butler, A. Walsh, *APL Mater.,* 2014, **2**, 081506.
18 A. Gómez, Q. Wang, A. R. Goñi, M. Campoy-Quiles, A. Abate, *Energy Environ. Sci.,* 2019, **12**, 2537-2547.
19 Y. Liu, L. Collins, R. Proksch, S. Kim, B. R. Watson, B. Doughty, T. R. Calhoun, M. Ahmadi, A. V. Ievlev, S. Jesse, S. T. Retterer, A. K. Belianinov, J. Huang, B. G. Sumpter, S. V. Kalinin, B. Hu, O. S. Ovchinnikova, *Nat. Mater.,* 2019, **18**, 1051-1053.
20 M. U. Rothmann, W. Li, Y. Zhu, U. Bach, L. Spiccia, J. Etheridge, Y. B. Cheng, *Nat. Commun.,* 2017, **8**, 14547.
21 E. Strelcov, Q. Dong, T. Li, S. J. Chae, Y. Deng, A. Gruverman, J. Huang, A. Centrone, *Sci. Adv.,* 2017, **3**, 1602165.
22 J. Beilsten-Edmands, G. E. Eperon, R. D. Johnson, H. J. P. G. SnaithRadaelli, *Appl. Phys. Lett.,* 2015, **106**, 173502.
23 Z. Fan, J. Xiao, K. Sun, L. Chen, Y. Hu, J. Ouyang, K. P. Ong, K. Zeng, J. Wang, *J Phys. Chem. Lett.,* 2015, **6**, 1155-1161.
24 I. M. Hermes, S. A. Bretschneider, V. W. Bergmann, D. Li, A. Klasen, J. Mars, W. Tremel, F. Laquai, H.-J. Butt, M. Mezger, R. Berger, B. J. Rodriguez, S. A. L. Weber, *J. Phys. Chem. C,* 2016, **120**, 5724-5731.
25 B. Huang, G. Kong, E. N. Esfahani, S. Chen, Q. Li, J. Yu, N. Xu, Y. Zhang, S. Xie, H. Wen, P. Gao, J. Zhao, J. Li, *npj Quantum Mater.,* 2018, **3**, 30.
26 Z. Xiao, Y. Yuan, Y. Shao, Q. Wang, Q. Dong, C. Bi, P. Sharma, Gruverman, Huang, J. A. *Nat. Mater.*, 2015, **14**, 193-198.
27 C. C. Stoumpos, C. D. Malliakas, M. G. Kanatzidis, *Inorg. Chem.,* 2013, **52**, 9019-9038.
28 Y. Dang, Y. Liu, Y. Sun, D. Yuan, X. Liu, W. Lu, G. Liu, H. Xia, X. Tao, *CrystEngComm,* 2015, *17*, 665-670.
29 A. W. Poglitsch, *J. Chem. Phys.,* 1987, **87**, 6373.
30 T. Baikie, Y. Fang, J. M. Kadro, M. Schreyer, F. Wei, S. G. Mhaisalkar, M. Graetzel, T. J. White, *J. Mater. Chem. A.,* 2013, **1**, 5628-5641.
31 M. T. Weller, O. J. Weber, P. F. Henry, A. M. Di Pumpo, T. C. Hansen, *Chem Commun,* 2015, **51**, 4180-4183.
32 R. Ohmann, L. K. Ono, H. S. Kim, H. Lin, M. V. Lee, Y. Li, N. G. Park, Y. Qi, *J. Am. Chem. Soc,.* 2015, **137**, 16049-16054.
33 Z. R. Gao, X. F. Sun, Y. Y. Wu, Y. Z. Wu, H. L. Cai, X. S. Wu, *J. Phys. Chem. Lett.,* 2019, **10**, 2522-2527.
34 M. Simenas, S. Balciu Nas, M. Maczka, J. R. Banys, E. E. Tornau, *J. Phys. Chem. Lett.,* 2017, **8**, 4906-4911.
35 I. Anusca, S. Balčiūnas, P. Gemeiner, Š. Svirskas, M. Sanlialp, G. Lackner, C. Fettkenhauer, J. Belovickis, V. Samulionis, M. Ivanov, B. Dkhil, J. Banys, V. V. Shvartsman, D. C. Lupascu, *Adv. Energy Mater*., 2017, **7**, 1700600.
36 C. Motta, F. El-Mellouhi, S. Kais, N. Tabet, F. Alharbi, S. Sanvito, *Nat. Commun.,* 2015, **6**, 7026.
37 J. H. Lee, N. C. Bristowe, P. D. Bristowe, A. K. Cheetham, *Chem. Commun.,* 2015, **51**, 6434-6437.
38 Y. Fang, H. Wei, Q. Dong, J. Huang, *Nat. Commun.,* 2017, **8**, 14417.
39 T. Baikie, N. S. Barrow, Y. Fang, P. J. Keenan, P. R. Slater, R. O. Piltz, M. Gutmann, S. G. Mhaisalkar, T. J. White, *J. Mater. Chem. A,* 2015, **3**, 9298-9307.
40 I. P. Swainson, R. P. Hammond, C. Soullière, O. Knop, W. Massa, *J. Solid State Chem.,* 2003, **176**, 97-104.
41 P. S. Whitfield, N. Herron, W. E. Guise, K. Page, Y. Q. Cheng, I. Milas, M. K. Crawford, *Sci. Rep.,* 2016, **6**, 35685.
42 A. Bernasconi, L. Malavasi, *ACS Energy Lett.,* 2017, **2**, 863-868.
43 M. Bari, A. A. Bokovand Z.-G. Ye. *J. Mater. Chem. C*, 2020, **8**, 9625-9631.
44 O. Knop, R. R. Wasylishen, M. A. White, T. S. Cameron, and M. J. M. Van Oort, *Can. J. Chem.,* 1990, **68**, 412-422.
45 R. E. Wasylishen, O. Knop, J. B. Macdonald, *Solid State Commun.,* 1985, **56**, 581−582.
46 N. Onoda-Yamamuro, T. Matsuo, H. Suga, *J. Phys. Chem. Solids,* 1992, **53**, 935–939.
47 Y. Guo, O. Yaffe, D. W. Paley, A. N. Beecher, T. D. Hull, G. Szpak, J. S. Owen, L. E. M. A. Brus, Pimenta, *Phys. Rev. Mater,* 2017, **1**, 042401.
48 K. Nakada, Y. Matsumoto, Y. Shimoi, K. Yamada, Y. Furukawa, *Molecules,* 2019, **24**, 626.
49 I. P. Swainson, C. Stock, S. F. Parker, L. Van Eijck, M. Russina, J. Taylor, W. *Phys. Rev. B,* 2015, **92**, 100303.
50 K. L. Brown, S. F. Parker, I. R. García, S. Mukhopadhyay, V. G. Sakai, C. Stock, *Phys. Rev. B., 2017*, **96,** 174111.
51 K. H. Wang, L. C. Li, M. Shellaiah, K. Wen Sun, *Sci. Rep.,* 2017, **7**, 13643.
52 H. Mashiyama, Y. Kurihara, *J. Korean Phys. Soc.,* 1998, **32**, 156-158.
53 Y. Kawamura, H. Mashiyama, *J. Korean Phys. Soc.,* 1999, **35**, 1437-1440.
54 S. G, P. Mahale, B. P. Kore, S. Mukherjee, M. S. Pavan, C. De, S. Ghara, A. Sundaresan, A. Pandey, T. N. Guru Row, D. D. Sarma, *J. Phys. Chem. Lett.,* 2016, **7**, 2412-2419.
55 Y. Kawamura, H. Mashiyama, K.Hasebe *J. Phys. Soc. Japan,* 2002, **71**, 1694-1697.
56 P. Zhao, J. Xu, X. Dong, L. Wang, W. Ren, L. Bian, A.Chang, *J. Phys. Chem. Lett.,* 2015, **6**, 2622-2628.
57 H. Mashiyama, Y. Kawamura. *J. Korean Phys. Soc.,* 2003, **42,** 1026-1029.
58 H. Mashiyama, Y. Kawamura, *J. Korean Phys. Soc.,* 2007, **51**, 850 -853.
59 L. Chi, I. Swainson, L. Cranswick, J.-H. Her, P. Stephens, O. Knop, *J. Solid State Chem.,* 2005, **178**, 1376-1385.
60 P. Nandi, C. Giri, D. Swain, U. Manju, D. Topwal, *CrystEngComm,* 2019, **21**, 656-661.

61 J. Sapriel, *Phys. Rev. B.,* 1975, **12**, 5128-5140.
62 A. A. Bokov, X. Long, Z.-G. Ye, *Phys. Rev. B.,* 2010, **81**, 172103.
63 E. Hartman, *An Introduction to Crystal Physics, International Union of Crystallography*, Cardiff, UK: Cardiff Press, 1984.
64 N. Onoda-Yamamuro, T. Matsuo and H. Suga, *J. Phys. Chem. Solids*., 1990, **51**, 1383-1395.
65 A. Pisoni, J. Jaćimović, O. S. Barišić, M. Spina, R. Gaál, L. Forró and E. Horváth, *J. Phys. Chem. Lett*., 2014, **5**, 2488–2492.
66 R. Heiderhoff, T. Haeger, N. Pourdavoud, T. Hu, M. Al-Khafaji, A. Mayer, Yi. Chen, H.-C. Scheer and T. Riedl, *J. Phys. Chem. C,* 2017, **121**, 28306–28311.
67 S. Zandi, P. Saxena, N. E. Gorji, *Sol. Energy,* 2020, **197**, 105-110.
68 L. Zhao, K. Roh, S. Kacmoli, K. A. Kurdi, S. Jhulki, S. Barlow, S. R. Marder, C. Gmachl, and B. P. Rand, *Adv. Mater.,* 2020, **32**, 2000752.
69 H. Kim, L. Zhao, J. S. Price, A. J. Grede, K. Roh, A. N. Bridgeman, M. Lopez, B. P. Rand & N. C. Giebink, *Nat. commun.,* 2018, **9**, 4893.
70 W. B. Gunnarsson and B. P. Rand, *APL Mater*., 2020, **8**, 030902.
71 L. Zhao, J. Gao, Y. L. Lin, Y.-W. Yeh, K. M. Lee, N. Yao, Y.-L. Loo and B. P. Rand, *Adv. Mater*., 2017, **29**, 1605317.
72 E. K. H. Salje, *Contemp. Phys.,* 2010, **41**, 79-91.
73 E. K. Salje, *Chemphyschem,* 2010, **11**, 940-950.
74 D. D. Viehland, E. K. H. Salje, *Adv. Phys.,* 2014, **63**, 267-326.
75 V. Y. Shur, A. R. Akhmatkhanov, I. S. Baturin, *Appl. Phys. Rev.,* 2015, **2**, 040604.
76 Y. Liu, M. Li, M. Wang, L. Collins, A. V. Ievlev, S. Jesse, K. Xiao, B. Hu, A. Belianinov, and O. S. Ovchinnikova, *APL Mater*., 2020, **8**, 011106.
77 X. Xiao, W. Li, Y. Fang, Y. Liu, Y. Shao, S. Yang, J. Zhao, X. Dai, R. Zia & J. Huang, *Nat. Commun.,* 2020, **11**, 2215.
78 J. Zhao, J. Y. Deng, H. Wei, X. Zheng, Z. Yu, Y. Shao, J. E. Shield, J. Huan, *Sci. Adv*., 2017, **3**, eaao5616.
79 Y. Liu, A. V. Ievlev, L. Collins, A. Belianinov, J. K. Keum, M. Ahmadi, S.n Jesse, S. T. Retterer, K. Xiao, J. Huang, B.G. Sumpter, S. V. Kalinin, B. Hu, and O. S. Ovchinnikova. *Adv. Electron. Mater.,* 2020, **6**. 1901235.

Keywords: Hybrid halide perovskites, Ferroelastic domain structure, Crystal symmetry, Phase transitions, Methylammonium lead bromide